MANGANESE OXIDE AEROGELS OBTAINED IN A ONE-STEP PROCESS DIRECTLY IN SUPERCRITICAL CO_2 AT DIFFERENT TEMPERATURES

Cite this: *INEOS OPEN*, **2021**, *4 (3)*, 112–116
DOI: 10.32931/io2115a

Received 14 July 2021,
Accepted 23 September 2021

http://ineosopen.org

I. V. Elmanovich[a,b]* and V. V. Zefirov[a,b]

[a] *Nesmeyanov Institute of Organoelement Compounds, Russian Academy of Sciences, ul. Vavilova 28, Moscow, 119991 Russia*
[b] *Faculty of Physics, Lomonosov Moscow State University, Leninskie Gory 1, str. 2, Moscow, 119991 Russia*

Abstract

The work presents a study of the formation of manganese oxide aerogels in the process of thermal decomposition of manganese carbonyls in oxygen-enriched supercritical CO_2 at different temperatures. The morphology of the aerogels was studied by means of electron microscopy; the porous structure was investigated through the analysis of low-temperature nitrogen adsorption/desorption isotherms. The process was observed in an optical high-pressure view-cell.

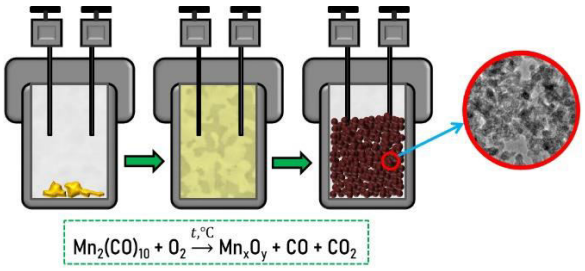

Key words: manganese oxide aerogels, supercritical CO_2, Brunauer–Emmett–Teller analysis, optical view-cell.

Introduction

Metal oxides in the form of dispersed nanoscale particles or networked structures are of tremendous interest for a wide variety of applications such as (electro)catalytic materials [1], sensors [2], or sorbents [3, 4]. Metal oxide aerogels, in that regard, provide a unique combination of extremely low density and high surface area. The approaches to the synthesis of metal oxide aerogels, first obtained by S. Kistler in his pioneering work [5, 6], can be divided into several generations. The work of S. Kistler featured alumina, ferric oxide, tungsten oxide and stannic oxide aerogels synthesized using the corresponding metal salts as precursors. It was already clear that when metal salts are used as gel precursors, the control over the medium pH during the transition from di- and tetramers to multidimensional structures is an extremely nontrivial task. For example, the reaction of iron oxide gel formation described in Ref. [6] included the stage of dialysis of the solution during the course of 4 weeks. The time-consuming and resource-intensive nature of such synthesis stimulated a transition from metal salts to alkoxides of the corresponding metals as precursors [7]. This transition allowed one to decrease the time required for the synthesis, which marks the second stage of research in the field of metal oxide aerogels. However, difficulties in obtaining the precursors themselves—metal alkoxides with sufficient stability towards hydrolysis—required further development and new approaches. The work of Prof. Alexander Gash that describes the gelation of metal salts using epoxides as proton "scavengers" initiated the next generation of research [8]. The "epoxy-initiated gelation" developed by A. Gash was a true breakthrough in the field, allowing for the synthesis of mechanically stable aerogels of oxides of various metals with high specific surface areas and low densities [9–13]. Moreover, it has been shown that the epoxide structure directly affects the nucleation and growth of aerogels, which provides an excellent opportunity for the synthesis of materials with tuned micro- and macro-properties. For iron oxide aerogels obtained *via* epoxy-initiated gelation, it was demonstrated that the structures of different types (globules and fibrils) can be obtained by varying the chemical structure of the epoxide and, consequently, the reaction rate [12].

Nevertheless, the process of obtaining aerogels remained multistage since it involved, among others, separate stages for solvent replacement and drying. The most widely used drying techniques include ambient drying, freeze-drying, and supercritical drying. The latter implies the use of a supercritical fluid (usually supercritical CO_2) to replace a liquid solvent of the gel with the subsequent removal of the supercritical solvent *via* its isothermal expansion. Supercritical drying procedure leads to the efficient preservation of the original three-dimensional structure of the gel. Currently, one-stage sol-gel reactions that proceed directly in supercritical CO_2 (sc CO_2) are of particular interest as an approach that can initiate yet another generation of studies of metal oxide aerogels and expand the possibilities of their industrial application [14]. Indeed, the formation of a gel directly in sc CO_2 allows one to eliminate time-consuming solvent replacement and drying procedures: the aerogel is formed in this case simply by the virtue of decompressing the reactor. In most cases, such a sol-gel process is carried out either in water/sc CO_2 microemulsions ("nanoreactors") stabilized with suitable surfactants [15–17] or in sc CO_2 with the addition of anhydrous acids [18–20]. The use of multicomponent systems, especially those that include compounds liquid under normal conditions, may not be optimal when scaling up the synthesis in sc CO_2. The presence of a residual amount of the additives such as surfactants or acids in the pores of aerogels might lead to the destruction of the porous structure of the material due to the collapse of the pores under the action of capillary effects. Thus, an additional stage of purification of the obtained materials will be required.

Three-dimensional aerogel-like metal oxide structures can be formed in oxygen-enriched sc CO_2 during thermal decomposition of corresponding metal carbonyls [21, 22]. The decomposition of manganese carbonyl and iron carbonyl yielded monolithic porous structures that completely filled the inner volume of the high-pressure vessel where they were prepared. These manganese oxide and iron oxide aerogel-like structures demonstrated the specific surface areas of 130 m^2/g and 70 m^2/g, respectively. The concentration of $Mn_2(CO)_{10}$ in the supercritical solution was directly proportional to both the size of MnO_x nanoparticles and the specific surface area of the aerogel [21]. Upon thermal decomposition in oxygen-enriched CO_2, cobalt and tungsten carbonyls formed dispersed nanoparticles with sizes ranging from 5 nm to 25 nm and with a strong tendency to agglomerate into branched 3D-structures [22]. It is important to note that this tendency to form branched nanoparticle structures during decomposition in sc CO_2 seems to be unique to metal carbonyls, for it was not observed for other organometallic precursors [23, 24]. This might be due to some specific interactions of carbonyl groups with CO_2 that provide nanoparticles growth stabilization. Among the studied metal oxide aerogels (MnO_x, FeO_x, CoO_x, WO_x) obtained in the process under discussion, MnO_x aerogels have the strongest tendency to form monolithic structures and the highest surface area. Therefore, they were chosen as the object of this research.

Here we propose a study of the dependence of manganese oxide aerogels properties, such as nanoparticles size, specific surface area, and volume of mesopores, on the temperature of decomposition in oxygen-enriched sc CO_2. We believe that the presented research is a necessary step in the investigation of the new approach, which might ultimately allow one both to obtain a deeper knowledge of the nucleation and growth of nanoparticles of metal oxides in sc CO_2 and to optimize the promising one-stage process or metal oxide aerogel preparation proposed by the research team.

Results and discussion

The manganese oxide aerogels were obtained in the process of thermal decomposition of manganese carbonyl in oxygen-enriched sc CO_2 at 95 °C, 100 °C, 105 °C, and 110 °C. The temperature range correlates with the temperature range of thermal decomposition of $Mn_2(CO)_{10}$ described in our previous work [22]. All the obtained manganese oxide aerogels were light-brown monolithic materials that occupied the entire volume of a high-pressure vessel. The appearance of the aerogels both inside the reaction and after the removal from the reactor was identical to that described in our previous works [21, 22]. Considering the precursor concentration, we can estimate that, before the removal of the materials from the high-pressure vessel, their density did not exceed $4 \cdot 10^{-3}$ g/cm^3. When the aerogel is removed from the vessel, considerable shrinkage occurs with an increase of the density by an order of magnitude: the resulting density is estimated to be up to $5 \cdot 10^{-2}$ g/cm^3, which is still well within the range of aerogels densities.

It is quite reliably established [25–27] that the thermal decomposition of manganese carbonyl $Mn_2(CO)_{10}$ occurs by homolytic decomposition of the molecule into two radicals $\cdot Mn(CO)_5$, which quickly lose carbonyl groups upon heating. In general terms, this can be written as follows: $Mn_2(CO)_{10} \rightarrow 2\,Mn(CO)_5 \rightarrow 2Mn + 10(CO)$ [28]. In the presence of oxygen in the system, its molecules can react with $Mn(CO)_5$, forming $(CO)_5MnO_2\cdot$ radical [29], the reaction using, in turn, can lead to the formation of $(CO)_5Mn–O–O–Mn(CO)_5$ complex. In this case, we assume that these complexes do not lose solubility in sc CO_2 (due to the presence of carbonyl groups), which allows the formation of a three-dimensional structure of aerogels. Further, the separation of carbonyl groups occurs, and some of them may be replaced by oxygen, which can result in the oxides of various stoichiometric compositions. In addition, in the presence of manganese oxide, oxygen can also oxidize the released CO molecules to CO_2 [30]. Thus, in general terms, the chemical reaction of aerogel formation can be presented as follows: $Mn_2(CO)_{10} + O_2 \xrightarrow{t,°C} Mn_xO_y + CO + CO_2$.

The typical TEM images of the MnO_x aerogels obtained at different temperatures are presented in Fig. 1. At the lower magnification (left column in Fig. 1), one can see that the aerogels are comprised of globule-like structural units. The sizes of the globules are in the range of 2–12 nm. Although a certain slight increase in the particle sizes with s decrease in the temperature (especially noticeable when comparing the images for Mn_110 and Mn_95 in Fig. 1) appears to be present, it is very hard to reliably establish this quantitatively due to the uneven shapes of the globule-like structural units. At the higher magnifications (right column in Fig. 1), the partial crystallinity of the aerogels is evident: for all the samples the images show areas with the ordered arrangement. However, no peaks can be observed on the corresponding XRD patterns (Fig. 2), probably due to the low crystallinity level and small crystallite sizes. The XRD study also demonstrates that the initial manganese carbonyl precursor with high crystallinity is absent from the reaction products.

For a more detailed study of the porous structure of the obtained aerogels, the isotherms of low-temperature adsorption/desorption of nitrogen were analyzed. The corresponding isotherms are presented in Fig. 3. For all the aerogels, the isotherms are of type IV according to the classification from Ref. [31]: adsorption at low relative pressure indicative of the presence of micropores is followed by a linear adsorption slope at P/P_0 in the range of 0.1–0.8 with the subsequent condensation at relative pressures of 0.8–1.0. The adsorption and desorption curves form hysteresis at P/P_0 = 0.8–1.0 (more prominent for Mn_Ox_110 and MnOx_105) due to the capillary condensation of nitrogen in the mesopores. The results of the Brunauer–Emmett–Teller (BET) analysis of the isotherms are given in Table 1. One can see from both the general view of the isotherms and the S_{BET} values that at temperatures above 100 °C (for Mn_Ox_105 and Mn_Ox_110 samples) there is an apparent correlation between the surface area and the temperature of the synthesis. We attribute this correlation to the dependence of the kinetics of nucleation and growth of manganese oxide nanoparticles on the temperature. Additionally, the incomplete conversion of the precursor at the lower temperatures can hinder the nitrogen adsorption and lead to the lower specific surface area and pore volume values.

The influence of the temperature of the synthesis on the porous structure of the aerogels is also confirmed by the Barrett-Joyner-Halenda (BJH) analysis of the isotherms. The pore size distributions derived from the BJH analysis are presented in Fig.

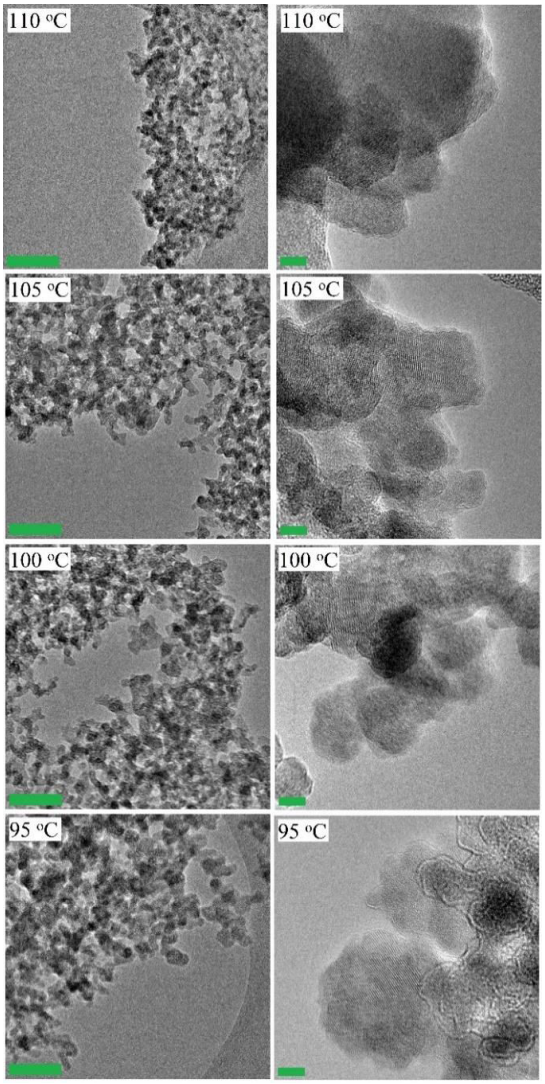

Figure 1. TEM images of the manganese oxide aerogels obtained at different temperatures. Scale bar in the left column – 50 nm, scale bar in the right column – 5 nm.

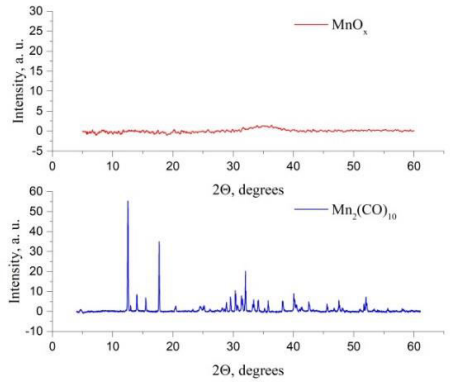

Figure 2. Bottom image: XRD patterns for $Mn_2(CO)_{10}$, top image: typical XRD image for MnO_x.

4; the values of specific surface area and pore volume of mesopores (IUPAC nomenclature) are given in Table 1. These values for the samples of Mn_Ox_95 and Mn_Ox_100 coincide within the margin of error, while at the temperatures above 100 °C (for Mn_Ox_105 and Mn_Ox_110) both S_{meso} and V_{meso} increase with a temperature rise.

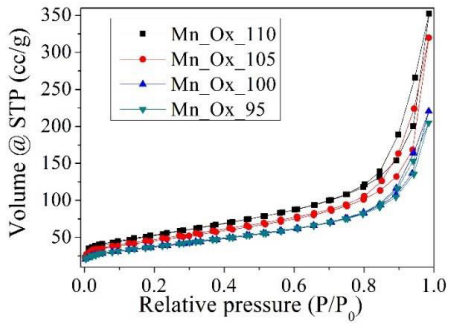

Figure 3. Low-temperature nitrogen adsorption isotherms for the manganese oxide aerogels obtained at different temperatures.

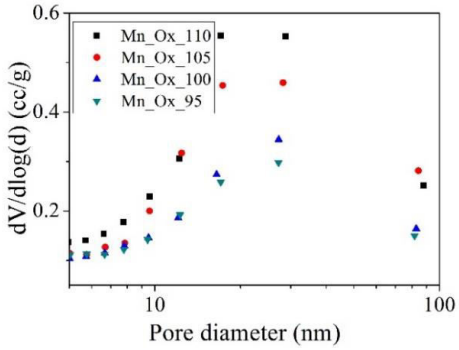

Figure 4. Pore size distribution of the manganese oxide aerogels obtained at different temperatures.

Table 1. The porous structure parameters of the obtained aerogels: specific surface area derived from the multipoint BET analysis; (S_{BET}) specific surface area (S_{meso}) and pore volume (V_{meso}) of mesopores derived from the BJH analysis

Sample	S_{BET}, m²/g	S_{meso}, m²/g	V_{meso}, cm^3/g
Mn_Ox_110	189	123	0.51
Mn_Ox_105	161	106	0.46
Mn_Ox_100	132	81	0.31
Mn_Ox_95	133	80	0.31

The proposed aerogel synthesis process at 100 °C was observed using a high-pressure optical view-cell with a large sapphire window (5 cm in radius). Figure 5 shows the photographs of the gel aging process. A top row of the images shows how CO_2 fills the reactor and easily dissolves the precursor. It is clearly seen that the precursor begins to dissolve even in the CO_2 gas phase. The reactor is filled with CO_2 at 35 °C to a pressure of 80 bar, with these parameters carbon dioxide is already in a supercritical state. Then, the gradual heating of the system begins (the second row of the images in Fig. 5). It is clearly seen that noticeable changes in the system begin when 90 °C is reached. When 100 °C is reached, the heating stops and the system is exposed for a specified time (the third row of the images in Fig. 4). In this case, the thermal decomposition of the precursor and nucleation of nanoparticles of manganese oxides are observed throughout the volume of the cell. However, no noticeable precipitation of the oxide phase is observed. In a little over an hour, the medium inside the reactor becomes completely impermeable to light but, then, the gradual precipitation of the formed nanoparticles starts and the

simultaneous "clearing" of the optical cell begins. The well-distinguishable individual agglomerates of nanoparticles are formed on sapphire glass. Similar agglomerates can be seen in the volume of the reactor: over time, they gradually sink to the bottom. As a result, in 10 h after the synthesis beginning (and approximately in 8 h after the precipitation start), there is a significant "clearing" of the medium inside the optical cell, associated with the precipitation of the formed nanoparticles. At the same time, it can be seen that a monolithic aerogel has not formed inside, but only its individual fragments. Additionally, during the process, we observed that the growth of the solid phase is concentrated in the vicinity of the stainless-steel walls of the reactor. Among the possible reasons for that localization, we can outline the heat transfer issues along with the possible catalytic effects of stainless-steel walls of the optical cell. In a standard synthesis procedure, the metal walls occupy almost the entire area bounding the synthesis zone. In the case of an optical cell, there are only thin metal regions inside the cell, while most of the area is occupied by sapphire windows, which can affect the synthesis process. Nevertheless, the visualized process illustrates in detail the main stages of aerogel synthesis as well as provides some useful tips for possible future scaling of the process.

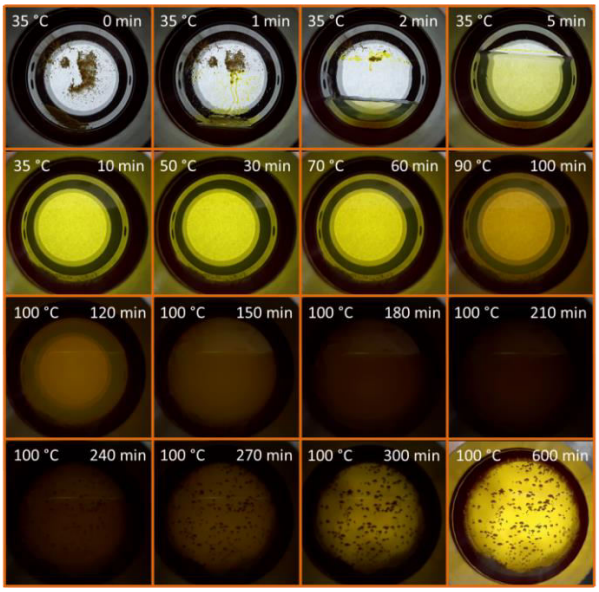

Figure 5. Photographs of all stages of the aerogel synthesis obtained using a high-pressure optical cell. Glass radius 5 cm.

Experimental

The general procedure for obtaining manganese oxide aerogels was adopted from our previous works where it was described in detail [21, 22]. Briefly, 100 mg of decacarbonyl dimanganese(0) (Sigma-Aldrich, 245267) was placed inside a high pressure vessel with an inner volume of 23 mL. The vessel was sealed and filled with oxygen to a pressure of 10 atm. The vessel was then placed in a thermostat at 40 °C and filled with CO_2 to a pressure of 100 atm to reach the density of 0.64 g/mL. The temperature of the thermostat was then raised to a certain reaction temperature. The reaction temperatures of 95 °C, 100 °C, 100 °C, and 105 °C were used. According to the NIST Chemistry WebBook program (National Institute of Standards and Technology, USA), the corresponding CO_2 pressure in the vessel was 264, 279, 295, and 310 atm, respectively. The synthesis took place within 24 h, after which the vessel was slowly decompressed and the resulting material was removed. All the samples obtained were monolithic aerogel structures. The resulting manganese oxide aerogels are marked as Mn_Ox_95, Mn_Ox_100, Mn_Ox_105, and Mn_Ox_110.

The phase composition of the materials was studied using X-ray diffraction (XRD). The powder X-ray diffraction patterns of the samples were obtained in a reflection geometry. The experiments were carried out on a Rigaku Smartlab SE diffractometer (Japan). The experimental patterns were obtained using CuKα radiation in a step scan mode with the step $\Delta 2\theta$ = 0.05° in the range of 2θ = 10°–90°.

To study the morphology of the samples, the TEM images were obtained using a JEOL JEM-2100F transmission electron microscope (Japan) operated at 200 kV. The low-temperature nitrogen adsorption/desorption study was performed on a Nova Station A instrument (Quantachrome Instruments, USA). Before isotherm measurements, all samples were kept under vacuum at 80 °C for 4 h. The isotherms were recorded at 77 K.

A specially designed high-pressure optical cell was used to visualize the synthesis process. It used uniquely large sapphire glasses with a radius of 5 cm. The total volume of the cell was 50 mL. During the experiment, the cell was filled with a sample of 140 mg of the precursor, hermetically sealed, then, 10 bar of oxygen and 80 bar of carbon dioxide were injected there at a temperature of 35 °C. Then the cell was slowly heated to a temperature of 100 °C and exposed for 10 h. During the entire process, the photographs were taken of the cell, illuminated from one side with a diode lamp.

Conclusions

The influence of the reaction temperature on the morphology and porosity of the manganese oxide aerogels was investigated. The study of the aerogels by means of TEM reveals that all the aerogels obtained at the temperatures from 95 °C to 110 °C were comprised of globule-like structures with the sizes ranging from 2 nm to 12 nm with even smaller sub-nanometer grains visible at the higher magnification. Although the crystallites are visible on the TEM images for all the obtained aerogels, the corresponding XRD patterns demonstrate no pronounced peaks, which is attributed to a combination of small crystallite sizes and a low degree of crystallinity. The results of the low-temperature nitrogen adsorption/desorption isotherm analysis revealed that starting from the temperature range (100–105) °C, SSA increases with temperature from 132 m^2/g at 100 °C to 189 m^2/g at 110 °C.

Acknowledgements

This work was supported by the Ministry of Science and Higher Education of the Russian Federation.

The authors are grateful to S. V. Maksimov (Chemistry Department, Moscow State University) for TEM measurements performed using MSU Chemistry Department "Nanochemistry and Nanomaterials" Equipment Center supported by Lomonosov Moscow State University Program of Development.

Corresponding author

* E-mail: elmanovich@polly.phys.msu.ru (I. V. Elmanovich)

References

1. A. Akbari, M. Amini, A. Tarassoli, B. Eftekhari-Sis, *Nano-Struct. Nano-Objects*, **2018**, *14*, 19–48. DOI: 10.1016/j.nanoso.2018.01.006
2. E. Fazio, S. Spadaro, C. Corsaro, G. Neri, S. G. Leonardi, F. Neri, N. Lavanya, C. Sekar, N. Donato, G. Neri, *Sensors*, **2021**, *21*, 2494. DOI: 10.3390/s21072494
3. H. Tian, J. Wu, W. Zhang, S. Yang, F. Li, Y. Qi, R. Zhou, X. Qi, L. Zhao, X. Wang, *Chem. Eng. J.*, **2017**, *313*, 1051–1060. DOI: 10.1016/j.cej.2016.10.135
4. J. W. Long, J. M. Wallace, G. W. Peterson, K. Huynh, *ACS Appl. Mater. Interfaces*, **2016**, *8*, 1184–1193. DOI: 10.1021/acsami.5b09508
5. S. S. Kistler, *Nature*, **1931**, *127*, 741. DOI: 10.1038/127741a0
6. S. S. Kistler, *J. Phys. Chem.*, **1932**, *36*, 52–64. DOI: 10.1021/j150331a003
7. S. J. Teichner, G. A. Nicolaon, M. A. Vicarini, G. E. E. Gardes, *Adv. Colloid Interface Sci.*, **1976**, *5*, 245–273. DOI: 10.1016/0001-8686(76)80004-8
8. A. E. Gash, T. M. Tillotson, J. H. Satcher, Jr., J. F. Poco, L. W. Hrubesh, R. L. Simpson, *Chem. Mater.*, **2001**, *13*, 999–1007. DOI: 10.1021/cm0007611
9. B. J. Clapsaddle, B. Neumann, A. Wittstock, D. W. Sprehn, A. E. Gash, J. H. Satcher, Jr., R. L. Simpson, M. Bäumer, *J. Sol-Gel Sci. Technol.*, **2012**, *64*, 381–389. DOI: 10.1007/s10971-012-2868-6
10. T. F. Baumann, A. E. Gash, S. C. Chinn, A. M. Sawvel, R. S. Maxwell, J. H. Satcher, *Chem. Mater.*, **2005**, *17*, 395–401. DOI: 10.1021/cm048800m
11. A. E. Gash, T. M. Tillotson, J. H. Satcher, L. W. Hrubesh, R. L. Simpson, *J. Non-Cryst. Solids*, **2001**, *285*, 22–28. DOI: 10.1016/S0022-3093(01)00427-6
12. A. E. Gash, J. H. Satcher, R. L. Simpson, *Chem. Mater.*, **2003**, *15*, 3268–3275. DOI: 10.1021/cm034211p
13. *Aerogels Handbook,* M. A. Aegerter, N. Leventis, M. M. Koebel (Eds.), Springer, New York, **2011**.
14. R. Sui, P. Charpentier, *Chem. Rev.*, **2012**, *112*, 3057–3082. DOI: 10.1021/cr2000465
15. M. E. Tadros, C. L. J. Adkins, E. M. Russick, M. P. Youngman, *J. Supercrit. Fluids*, **1996**, *9*, 172–176. DOI: 10.1016/S0896-8446(96)90029-7
16. M. S. Lee, S. S. Park, G.-D. Lee, C.-S. Ju, S.-S. Hong, *Catal. Today*, **2005**, *101*, 283–290. DOI: 10.1016/j.cattod.2005.03.018
17. K. T. Lim, H. S. Hwang, W. Ryoo, K. P. Johnston, *Langmuir*, **2004**, *20*, 2466–2471. DOI: 10.1021/la035646u
18. D. A. Loy, E. M. Russick, S. A. Yamanaka, B. M. Baugher, K. J. Shea, *Chem. Mater.*, **1997**, *9*, 2264–2268. DOI: 10.1021/cm970326f
19. R. A. Lucky, P. A. Charpentier, *Adv. Mater.*, **2008**, *20*, 1755–1759. DOI: 10.1002/adma.200702287
20. R. Sui, A. S. Rizkalla, P. A. Charpentier, *Langmuir*, **2005**, *21*, 6150–6153. DOI: 10.1021/la0505972
21. V. V. Zefirov, I. V. Elmanovich, A. V. Pastukhov, E. P. Kharitonova, A. A. Korlyukov, M. O. Gallyamov, *J. Sol-Gel Sci. Technol.*, **2019**, *92*, 116–123. DOI: 10.1007/s10971-019-05092-2
22. I. V. Elmanovich, V. V. Zefirov, I. D. Glotov, V. E. Sizov, E. P. Kharitonova, A. A. Korlyukov, A. V. Pastukhov, M. O. Gallyamov, *J. Nanopart. Res.*, **2021**, *23*, 95. DOI: 10.1007/s11051-021-05138-z
23. I. V. Elmanovich, A. V. Naumkin, M. O. Gallyamov, A. R. Khokhlov, *J. Nanopart. Res.*, **2012**, *14*, 733. DOI: 10.1007/s11051-012-0733-8
24. V. V Zefirov, I. V Elmanovich, E. E. Levin, S. S. Abramchuk, E. P. Kharitonova, A. A. Khokhlov, M. S. Kondratenko, M. O. Gallyamov, *J. Mater. Sci.*, **2018**, *53*, 9449–9462. DOI: 10.1007/s10853-018-2242-3
25. L. M. Fillman, S. C. Tang, *Thermochim. Acta*, **1984**, *75*, 71–84. DOI: 10.1016/0040-6031(84)85008-X
26. J. P. Fawcett, A. Poe, K. R. Sharma, *J. Am. Chem. Soc.*, **1976**, *98*, 1401–1407. DOI: 10.1021/ja00422a020
27. D. R. Bidinosti, N. S. McIntyre, *Can. J. Chem.*, **1970**, *48*, 593–597. DOI: 10.1139/v70-097
28. D. Hopgood, A. J. Poë, *Chem. Commun.*, **1966**, 831–832. DOI: 10.1039/C19660000831
29. S. A. Fieldhouse, B. W. Fullam, G. W. Neilson, M. C. R. Symons, *J. Chem. Soc., Dalton Trans.*, **1974**, 567–569. DOI: 10.1039/dt9740000567
30. S. Dey, V. V. P. Kumar, *Curr. Res. Green Sustain. Chem.*, **2020**, *3*, 100012. DOI: 10.1016/j.crgsc.2020.100012
31. S. J. Gregg, K. S. W. Sing, *Adsorption, Surface Area, and Porosity*, *2nd ed.*, Acad. Press, London, New York, **1982**.